Supramolecular Route to Well-Ordered Metal Nanofoams

Ivana Vukovic,[†] Sergey Punzhin,[‡] Zorica Vukovic,[⊥] Patrick Onck,[§] Jeff Th. M. De Hosson,[‡] Gerrit ten Brinke,[†,*] and Katja Loos[†,*]

[†]Polymer Chemistry, [‡]Materials Science, and [§]Micromechanics of Materials, Zernike Institute for Advanced Materials, University of Groningen, Nijenborgh 4, 9747 AG Groningen, The Netherlands, and [⊥]ICTM-Center for Catalysis and Chemical Engineering, Njegoševa 12, 11000 Belgrade, Serbia

ABSTRACT Metal nanofoams with a porosity above 50% v/v have recently attracted great interest in materials science due to their interesting properties. We demonstrate a new straightforward route to prepare such nanofoams using diblock copolymer-based PS-*block*-P4VP(PDP) supramolecules that self-assemble into a bicontinuous gyroid morphology, consisting of PS network channels in a P4VP(PDP) matrix. After dissolving the PDP, the P4VP collapses onto the PS struts and a free-standing bicontinuous gyroid template of 50−100 μm thickness and interconnected, uniformly sized pores is formed. The hydrophilic P4VP corona facilitates the penetration of water-based plating reagents into the porous template and enables a successful metal deposition. After plating, the polymer is simply degraded by heating, resulting in a well-ordered inverse gyroid nickel foam. Essential to this approach is the removal of only one part of the matrix (*i.e.*, PDP). Therefore, the template accounts for 50% v/v or more. The porosity characteristics (amount, size of pores) can be tuned by selecting the appropriate copolymer and by adjusting the amount of PDP.

KEYWORDS: metal nanofoams · nanopores · diblock copolymers · supramolecules · metal plating

Nanoporous metal foams represent a new, very promising class of materials that combine the properties of metals, such as catalytic activity, thermal and electrical conductivity, and the properties of nanoporous materials: low relative density and high specific surface area. These unique properties allow nanoporous metal foams to be used for a large number of possible applications as, for example, high power density batteries, substitutes for platinum group catalysts, hydrogen storage materials, actuators, *etc.*[1]

In the case of actuators, charge is injected at the surfaces, resulting in the enhancement of surface stresses.[2,3] When charge is injected, a narrow space charge layer of atomic dimensions is formed at the surface. In this layer, the electronic density of states changes, which modifies the atomic bonding potentials. As a result, the surface layer tends to favor a lateral atomic spacing that differs from that of the bulk, creating a surface stress. Despite the limited size of space charge regions in metals due to the efficient electronic screening, it has been shown that these tunable surface stresses can be exploited in highly porous materials when the ligament (subunit) sizes are on the order of tens of nanometers.[4,5] This has recently led to a new class of actuators: nanoporous metals.[6] When immersed in an electrolyte, nanoporous metal expands and contracts reversibly if an external bias voltage is applied. An intriguing feature of nanoporous actuator materials is that the overall behavior is not a direct result of the electromechanical behavior of the nanoscale ligaments. Instead, the macroscopic functional properties emerge as a result of the interaction of individual subunits, which is strongly dictated by the topological information of the nanostructural architecture, that is, the morphology and connectivity of the nanoscale ligaments.

Dealloying,[7] sol−gel approaches,[8,9] and combustion synthesis[10] are commonly employed techniques to generate nanoporous metals. A characteristic property of these materials is that their nanocellular architecture is highly disordered. It is well-known from studies on the mechanical behavior of structural cellular metals and metallic foams that disordered architectures are not able to effectively transmit stresses from the ligament scale to the overall (macro) scale, resulting in poor mechanical properties.[11−13] In the present paper, we demonstrate how the unique self-assembly properties of block-copolymer-based supramolecules may be employed to synthesize nanoporous metals having a well-defined and ordered cellular architecture with porosities exceeding 50% v/v.

It is well-known that block copolymers, depending on the number of blocks, their chain length and flexibility, volume fraction, and the extent of repulsion between the chemically connected blocks, self-assemble into a variety of structures with internal length scales ranging from tens to hundreds or more nanometers.[14−16] The most common are

* Address correspondence to k.u.loos@rug.nl, g.ten.brinke@rug.nl.

Received for review April 18, 2011 and accepted July 8, 2011.

Published online July 08, 2011
10.1021/nn201421y

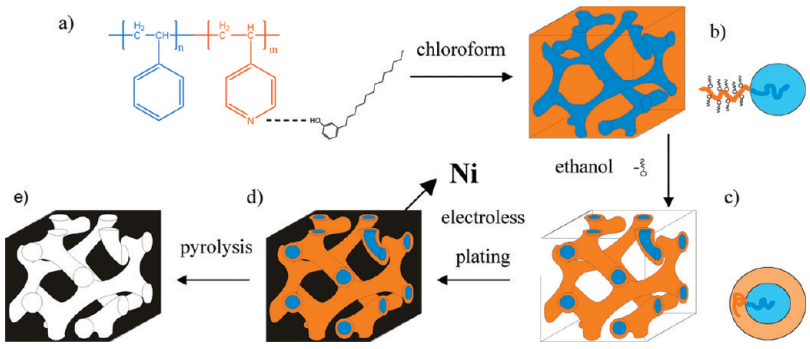

Figure 1. Schematic representation of the preparation of gyroid metallic nanofoam. (a) Chemical structure of the supramolecular complex PS-*b*-P4VP(PDP)$_x$. (b) Bicontinuous gyroid morphology of PS-*b*-P4VP(PDP)$_x$. (c) Nanoporous template after the PDP removal. (d) By electroless deposition, the voids between PS struts are filled with nickel. (e) Gyroid nickel nanofoam after the polymer template removal by pyrolysis.

body-centered cubic spheres, hexagonally ordered cylinders, and lamellar phase. Other morphologies, such as the bicontinuous gyroid and hexagonally perforated lamellae, are usually observed in the weak to intermediate segregation regime.[17,18] However, it has been reported recently that the bicontinuous gyroid morphology may also exist in the strong segregation regime, albeit in an even narrower region.[19−21] Increase in the number of blocks of the polymer chain and variation of the chain architecture lead to even more complex structures (see refs 16 and 22−27 and references therein).

Block copolymers containing chemically degradable blocks are versatile precursors to nanoporous materials.[28] Widely employed techniques to eliminate the targeted block from self-assembled block copolymers are etching,[29,30] hydrolysis,[31] and ozonolysis.[32,33] An attractive alternative is provided by self-assembled supramolecules, where nanoporous structures may be obtained by simple dissolution. Suitable block-copolymer-based supramolecules are obtained by hydrogen bonding side groups to one of the blocks of a diblock copolymer, which then are removed by a selective solvent after the self-assembly has taken place.[34,35] That the morphology of these systems can be tailored by a simple variation of the relative volume fraction of the side groups is an important additional asset of this approach.[36] The thus generated nanoporous materials retain the originally ordered morphology of the precursor and, consequently, provide ample opportunities for nanotechnological applications.[30,37,38] This approach is conceptually similar to the generation of nanoporous structures from diblock copolymer/homopolymer blends of polystyrene-*block*-polymethylmethacrylate and polymethylmethacrylate, PS-*b*-PMMA/PMMA, *via* selective removal of homopolymer PMMA by acetic acid.[39]

The cylindrical morphology can be, for instance, used as a template for the fabrication of nanowires, provided the cylinders have a perpendicular orientation to the substrate surface.[37,38] A way to create nanoporous structures that do not involve alignment issues is to use continuous morphologies.[30,40] Hashimoto *et al.* were the first to exploit the bicontinuous gyroid morphology for metal plating purposes.[41] They reported the formation of a nanoporous film by the ozonolysis of the minority phase (PI) in a gyroid forming PS-PI block copolymer/PS homopolymer blend. The nanochannels were subsequently coated with nickel. Following this, a number of studies on the preparation and potential application of gyroid-forming nanoporous structures have appeared.[30,42−44]

Here, we report a new method for a simple and robust preparation of well-ordered gyroid metallic nanofoams. Our procedure is summarized schematically in Figure 1. A supramolecular complex of PS-*b*-P4VP diblock copolymer and amphiphilic PDP was used as a precursor for the nanoporous template for subsequent metal plating. PDP molecules interact *via* hydrogen bonds with the pyridine rings to form a PS-*b*-P4VP(PDP)$_x$ complex (Figure 1a; the subscript x denotes the ratio between PDP molecules and P4VP repeat units). The block lengths of the block copolymer and the amount of PDP were selected in such a way that the self-assembly gave rise to a bicontinuous gyroid morphology with a PS network in a matrix of P4VP(PDP)$_x$ (Figure 1b). The PDP side chains were selectively removed in ethanol (Figure 1c), after which the P4VP chains collapsed onto the PS, thus forming a polar corona around the PS network struts. Subsequently, electroless deposition was performed such that the metal was distributed uniformly throughout the macroscopic thickness of the template (50−100 μm, Figure 1d). The metal nanofoam obtained after the removal of polymer template perserved the well-defined gyroid structure with long-range order (Figure 1e).

The value of the Flory−Huggins interaction parameter between polystyrene (PS) and poly(4-vinylpyridine) (P4VP) is on the order of $\chi_{S,4VP} \cong 0.35$.[45,46] This implies that a PS-*b*-P4VP diblock copolymer will be in the strong segregation limit except for small

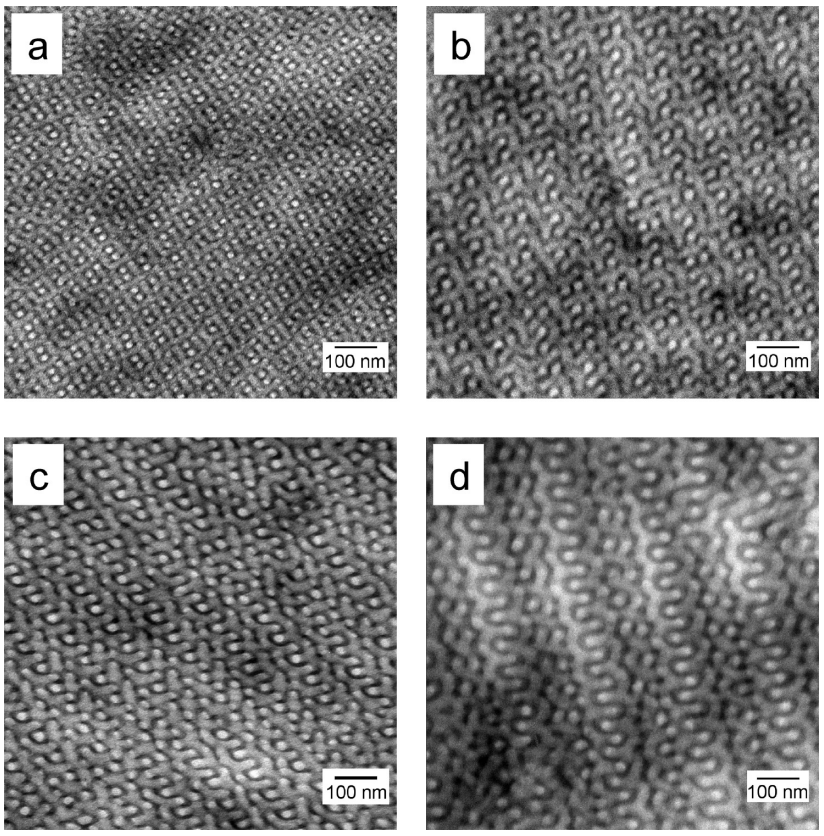

Figure 2. Bright-field TEM images representing the double-wave pattern: the projection through the gyroid (211) plane. The samples are PS-*b*-P4VP(PDP)$_x$ diblock copolymer complexes with the following characteristics: (a) $x = 1.0$, $f_{P4VP(PDP)} = 0.61$, $M_{total} = 61\,000$ g mol^{-1}; (b) $x = 1.0$, $f_{P4VP(PDP)} = 0.62$, $M_{total} = 83\,300$ g mol^{-1}; (c) $x = 0.8$, $f_{P4VP(PDP)} = 0.59$, $M_{total} = 90\,600$ g mol^{-1}; (d) $x = 1.5$, $f_{P4VP(PDP)} = 0.69$, $M_{total} = 135\,000$ g mol^{-1}. P4VP(PDP)$_x$ domains are dark due to the iodine staining.

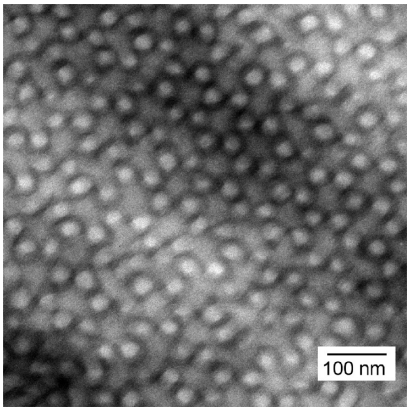

Figure 3. Bright-field TEM image representing the wagon-wheel pattern: the projection through the gyroid (111) plane. The sample is PS-*b*-P4VP(PDP)$_{1.5}$ diblock copolymer complex, $f_{P4VP(PDP)} = 0.69$, $M_{total} = 135\,000$ g mol^{-1}. P4VP-(PDP)$_{1.5}$ domains are dark due to the iodine staining.

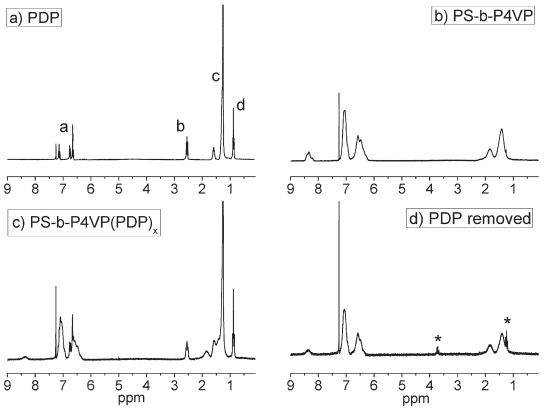

Figure 4. ^{1}H NMR of (a) PDP, (b) PS-*b*-P4VP diblock copolymer, (c) PS-*b*-P4VP(PDP)$_x$ supramolecular complex, and (d) PS-*b*-P4VP(PDP)$_x$ after washing with ethanol; the peaks marked with an asterisk are due to residual ethanol.

molar masses, which therefore diminishes the possibility of a bicontinuous gyroid self-assembly.[47] However, the addition of a small amphiphilic molecule, such as 3-pentadecylphenol (PDP), to PS-*b*-P4VP appears to reduce the effective interaction parameter between the two phases, PS and P4VP(PDP), respectively, as a series of lamellar self-assembled PS-*b*-P4VP(PDP)$_{1.0}$ systems showed a chain length dependence of the long period that is characteristic for the intermediate segregation regime.[48] This is also corroborated by the observation that a PS-*b*-P4VP(PDP)$_{1.0}$ complex, from a PS-*b*-P4VP diblock copolymer with block weight average molar masses of 19.3 and 5.1 kg mol^{-1}, respectively, becomes disordered above *ca.* 170 °C. The pure diblock copolymer, for which $\chi N \approx 80$, obviously remains ordered at all accessible temperatures.

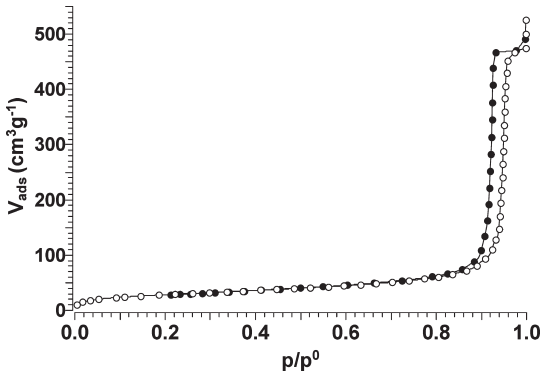

Figure 5. Nitrogen adsorption–desorption isotherm of the porous PS-*b*-P4VP(PDP)$_{1.0}$ film after ethanol treatment.

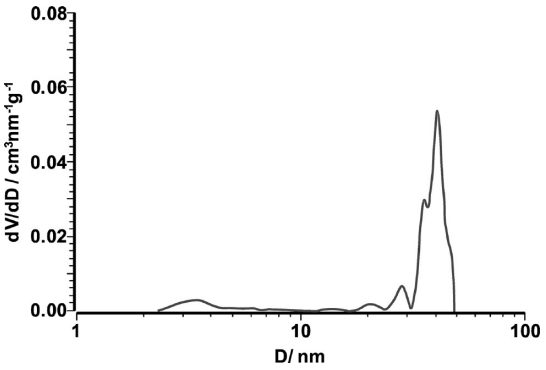

Figure 6. Pore size distribution of the porous PS-*b*-P4VP-(PDP)$_{1.0}$ film after ethanol treatment; the derivative of the cumulative pore volume curve *vs* pore diameter.

These complexes therefore have a higher probability for bicontinuous gyroid structure formation. Additives can as well stabilize structures that are not found in conventional diblock copolymers, such as plumber nightmare morphology,[49] but there are no indications that this also occurs in our supramolecular systems.[50]

It is very important to realize that the PS(core)–P4VP(corona) (Figure 1c) gyroid network occupies more than 50 vol %, and consequently, the porosity of the formed nanoporous metal foam (Figure 1e) is high enough to fulfill the general requirement for the formation of a metal nanofoam.[1] In contrast, the removal of the matrix-forming block from a conventional bicontinuous gyroid diblock copolymer structure would result in a highly porous template (porosity *ca.* 65 vol %) and a correspondingly far less porous (*ca.* 35 vol %) metal nanostructure.

Additionally, in a conventional diblock copolymer approach employing, for example, diblock copolymers of PS and polyethylene oxide (PEO) or polylactide (PLA),[40] the removal of the chemically degradable matrix (PLA or PEO) from the bicontinuous gyroid morphology results in a rather hydrophobic surface of PS, which usually requires surface modification for uniform metal deposition.[51] With the supramolecular approach presented here, this issue is overcome by the presence of the hydrophilic P4VP corona that facilitates the penetration of the water-based plating reagents into the porous template.

RESULTS AND DISCUSSION

Morphological Characterization of PS-*b*-P4VP(PDP)$_x$ Complexes. In principle, PS-*b*-P4VP(PDP)$_x$ complexes could form two different gyroid morphologies, one with PS as the minority phase forming the bicontinuous network in a P4VP(PDP)$_x$ matrix and the reverse system where the P4VP(PDP)$_x$ phase forms the bicontinuous network in a PS matrix. The former has indeed been observed for a specific PS-*b*-P4VP(PDP)$_x$ complex with x = 1.0 and a weight fraction of the comb block ($f_{P4VP(PDP)}$) 0.62.[50] The reverse structure has never been observed.

TABLE 1. Textural Properties of the Porous PS-*b*-P4VP(PDP)$_{1.0}$ Film after Ethanol Treatment Obtained from the Nitrogen Adsorption–Desorption Isotherm

S_{BET}, m^2 g^{-1}	$V_{p,0.99}$, mm^3 g^{-1}	$V_{p,total}$[a], mm^3 g^{-1}	D_{med}[a], nm	D_{max}[a], nm
104	795	715	39.8	40.8

[a] Cumulative pore volume $V_{p,total}$, median pore diameter D_{med}, and maximum pore diameter D_{max} are determined using the Dollimore and Heal method.

For the present study, different amounts of PDP ($0.5 \leq x \leq 1.5$) were added to a set of four different PS-*b*-P4VP diblock copolymers with a weight fraction of the P4VP block (f_{P4VP}) ranging from 0.28 to 0.30. The total molar mass of the supramolecular complexes did not exceed 150 kg mol^{-1}, and the weight fraction of the comb block ($f_{P4VP(PDP)}$) in the complexes varied from 0.50 to 0.69. A simple adjustment of the amount of PDP allowed us to prepare a series of supramolecular complexes with a bicontinuous gyroid morphology starting from these diblock copolymers. Similarly, the morphology of block copolymers can be manipulated by addition of homopolymer.[15]

The gyroid morphology of the PS-*b*-P4VP(PDP)$_x$ complexes in bulk was confirmed by TEM. Figure 2 shows representative bright-field TEM images of the iodine-stained ultrathin sections. The P4VP(PDP)$_x$ block domains appear dark because they are selectively stained with iodine due to the formation of a charge transfer complex. TEM images reveal the typical double-wave pattern that is known to represent the projection through the (211) plane of the gyroid unit cell. It becomes obvious that the periodicity for the selected systems increases with a factor of 3, from *ca.* 50 to *ca.* 150 nm. Figure 3 shows the wagon-wheel pattern that is characteristic for the gyroid (111) projection.

Generation and Characterization of the Porous Structure. By subjecting the film of the PS-*b*-P4VP(PDP)$_x$ complex to ethanol, the PDP side chains were selectively removed (Figure 1c). The complete removal of PDP was proven by ^{1}H NMR (Figure 4).

The signals characteristic for PDP are marked in Figure 4a. Figure 4c shows the spectrum of the

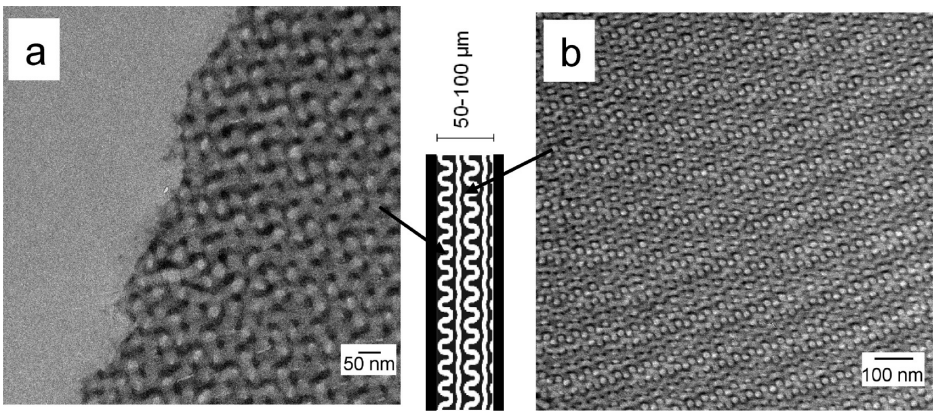

Figure 7. Bright-field TEM images of the unstained ultrathin-sectioned nickel-plated gyroid polymer template. The nickel-plated domains appear dark. The starting supramolecular complexes PS-*b*-P4VP(PDP)$_x$ have the following characteristics: x = 1.5, $f_{P4VP(PDP)}$ = 0.69, M_{total} = 135 000 g mol^{-1}. A schematic representation of the nickel-plated film is shown, as well. (a) Area located near the surface of the plated film; the epoxy resin used for embedding is visible in the left part of the image. (b) Area located in the middle of the plated film.

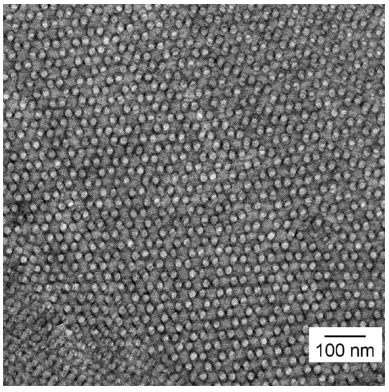

Figure 8. Bright-field TEM image of the unstained ultrathin-sectioned nickel-plated gyroid polymer template. The nickel-plated domains appear dark. The starting supramolecular complex PS-*b*-P4VP(PDP)$_x$ has the following characteristics: x = 1.0, $f_{P4VP(PDP)}$ = 0.62, M_{total} = 83 300 g mol^{-1}. The image represents the (111) gyroid projection.

supramolecular complex PS-*b*-P4VP(PDP)$_x$. As expected, it is simply the sum of PDP and diblock copolymer (Figure 4b) spectra, and the characteristic PDP peaks are visible. However, after the ethanol treatment (Figure 4d), the PDP peaks are absent and the spectrum of the diblock copolymer is recovered. This confirms that the ethanol washing provides the complete removal of PDP from the sample. The absence of PDP after the ethanol treatment was verified using DSC as well (Supporting Information, Figure 1). The DSC data furthermore indicate that the temperature of the subsequent nickel plating step should not exceed 105 °C because higher temperatures will most likely destroy the gyroid morphology.

By the complete PDP removal, the matrix of the complexes is emptied and a double PS (core)—P4VP (corona) network is exposed. A formation of large defects in the structure, a presence of closed or disconnected pores or even a complete collapse of the network are some of the apparent possibilities which can consequently disqualify this system as a precursor to nanoporous metal foams. Therefore, the textural properties of the porous PS-*b*-P4VP(PDP)$_{1.0}$ film ($f_{P4VP(PDP)}$ = 0.62 and M_{total} = 83 300 g mol^{-1} before the ethanol treatment) after the ethanol treatment were determined using the nitrogen adsorption—desorption isotherm. The nitrogen adsorption—desorption isotherm corresponds to the type IV isotherms according to the IUPAC classification (Figure 5). The initial part of the isotherm (at low relative pressure) is reversible, and it is attributed to a monolayer—multilayer adsorption of nitrogen onto the sample surface. At higher relative pressure, there is a hysteresis loop of the H1 type, which is associated with the capillary condensation in the mesopores and indicates cylindrical pore geometry and high degree of pore size uniformity. The shape of the adsoprtion isotherm at relative pressure near unity offers the possibility to determine the total pore volume, $V_{p,0.99}$, using the method given by Gurvitsch.[52,53] From the adsorption branch of the nitrogen isotherm, the distribution of the pore volume according to their size is calculated. The calculation is based on the Kelvin equation that correlates the relative equilibrium pressure to the pore diameter (allowance for the thickness of the adsorbed layer is made, and a cylindrical shape of the pores is assumed). The derivative of the cumulative pore volume with respect to the pore diameter for the porous PS-*b*-P4VP(PDP)$_{1.0}$ film after the ethanol treatment is shown in Figure 6. The data obtained are summarized in Table 1. The textural properties of the porous film were also determined by mercury porosimetry (Supporting Information, Figure 2, Table 1). Excellent agreement between the nitrogen adsorption and mercury porosimetry results is found. Additionally, mercury porosimetry was performed for one more sample, notably a porous PS-*b*-P4VP(PDP)$_{0.8}$ film ($f_{P4VP(PDP)}$ = 0.58 and M_{total} = 90 600 g mol^{-1} before the ethanol treatment, Supporting Information, Figure 3, Table 1).

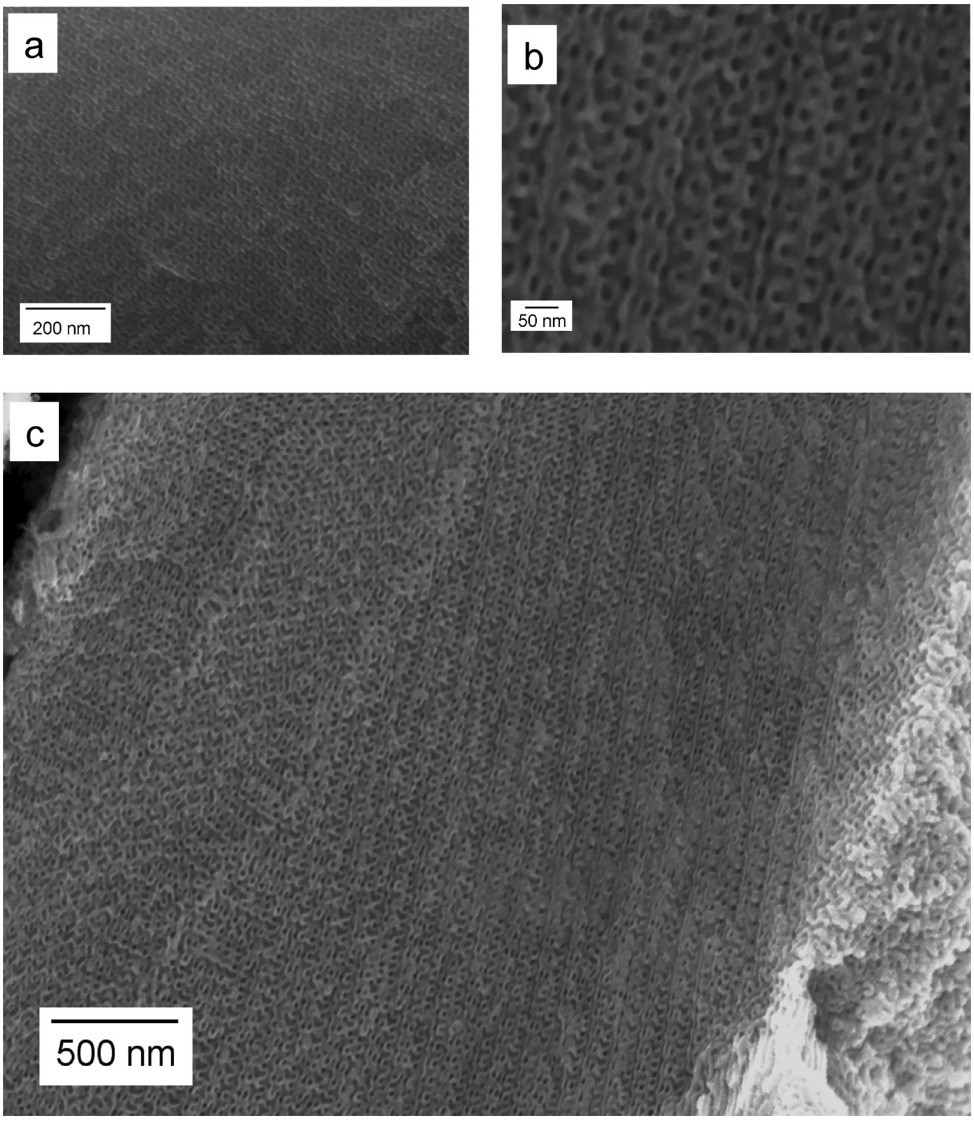

Figure 9. SEM images of the inverse gyroid nickel replicas obtained after the polymer template removal by pyrolysis (pyrolysis time = (a) 3 h; (b,c) 4 days). A 3D network structure composed of the interconnected nickel struts is clearly visible. The starting supramolecular complexes PS-*b*-P4VP(PDP)$_x$ have the following characteristics: (a) x = 1.0, $f_{P4VP(PDP)}$ = 0.62, M_{total} = 83 300 g mol^{-1}; (b,c) x = 1.5, $f_{P4VP(PDP)}$ = 0.69, M_{total} = 135 000 g mol^{-1}.

The data confirm the formation of a mesoporous structure with a very narrow pore size distribution. The average pore diameter of 40 nm is comparable to the size of the P4VP(PDP)$_{1.0}$ domain. The BET specific surface area is rather high and is determined to be 104 m^2 g^{-1}. The expected porosity of the PS-*b*-P4VP(PDP)$_{1.0}$ film after the ethanol treatment is calculated to be 46 vol % on the basis of the amount of PDP originally present using the approximation of equal bulk densities. From $V_{p,0.99}$ and $V_{p,total}$ determined using the nitrogen adsorption–desorption isotherm, the porosity of the template was evaluated to be 44.3 and 41.7 vol %, respectively, well below the 50% v/v as required for a template for the production of metal nanofoams.

Inserting Nickel in the Polymer Template. Electroless plating is employed to insert nickel in the pores of the gyroid polymer template (Figure 1d). This technique offers the possibility to create uniform coatings over complicated surfaces or to insert metal in complex-shaped nanochannels.[54,55] Another advantage over conventional electrochemical plating is that the surface of the template does not necessarily have to be conductive. The water-based plating reagents diffuse through the interconnected channels and influence sensitization and activation of their surface followed by nickel deposition onto the activated areas. The affinity between the aqueous plating solutions and the surface of the template is a very important factor for the successful nickel deposition.

In the pretreatment step, the catalyst Pd is deposited onto the surface of the gyroid network: PS core/P4VP corona. It directs selective nickel ion reduction at the activated surfaces. During the successive metal deposition, nickel fills the pores of the polymer

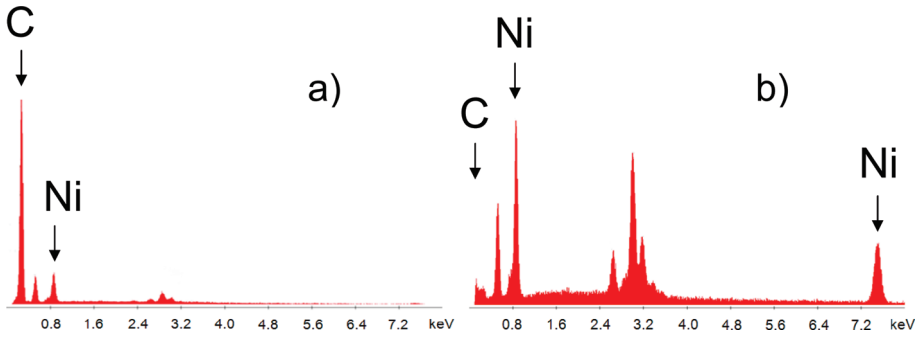

Figure 10. EDX analysis of the nickel-plated sample before (a) and after the polymer template removal (b). The starting supramolecular complex is PS-*b*-P4VP(PDP)$_{1.5}$, $f_{P4VP(PDP)}$ = 0.69, M_{total} = 135 000 g mol^{-1}. The peaks in the region of 2.40−4.00 keV in (b) originate from the silver paste that is used to attach the sample to the sample holder (Supporting Information, Figure 6).

template. Figure 7 shows the bright-field TEM images of ultrathin sections of the nickel-plated samples. The samples are not stained, and therefore, the contrast in the TEM images results from nickel deposited in the nanochannels. The observed TEM images are in good agreement with the TEM images of the supramolecular complexes: the dark nickel domains in Figure 7 correspond to the dark P4VP-(PDP)$_{1.0}$ domains stained with iodine in Figure 2. Figure 7a represents an area located near the surface of the plated film, while the middle of the plated film is shown in Figure 7b. Both pictures confirm the homogeneous distribution of nickel throughout the film. The characteristic wagon-wheel pattern of the (111) gyroid projection is shown in Figure 8 and further confirms the preservation of the double gyroid morphology during the PDP removal and the electroless nickel plating.

Exposure of the Inverse Gyroid Nickel Foam. Subsequently, the polymer template is decomposed by heating isothermally at 350 °C (Figure 1e), while leaving the nickel network intact. Thermogravimetric analyses of the porous PS-*b*-P4VP(PDP)$_x$ films following the PDP removal (Supporting Information, Figure 4) suggest a minimal pyrolysis time of 30 min. The nickel replica remains stable after the thermal treatment and retains the inverse gyroid morphology imposed by the structure of the porous polymer template, as evidenced by SEM images (Figure 9). Longer pyrolysis time, up to 4 days, does not affect the stability of nickel nanofoam (Figure 9b,c). Figure 9b reveals the typical gyroid double-wave pattern, and Figure 9c shows a micrometer-sized area of the gyroid ordering. Additional SEM images (Supporting Information, Figure 5) confirm the inverse gyroid morphology of the nanofoams obtained.

The chemical composition of the sample before and after pyrolysis is analyzed with energy-dispersive analysis of X-rays (EDX), and the result is shown in Figure 10. The dominant carbon peak in Figure 10a disappears after the thermal treatment of the sample (Figure 10b), which indicates the efficiency of the thermal treatment. In Figure 10b, the two prominent peaks correspond to nickel. An oxygen peak around 0.5 keV indicates the oxidation of the nickel nanofoam when stored in air.

CONCLUSION

Supramolecular PS-*b*-P4VP(PDP) complexes with a bicontinuous gyroid morphology were used as templates to produce metallic nickel nanofoams. The complete dissolution of PDP from the complex with the major P4VP(PDP) component forming the matrix results in an open network structure with struts consisting of a PS core and a P4VP corona. The high specific surface area and the narrow pore size distribution of the structure formed are evidenced by nitrogen adsorption and mercury porosimetry. The open nature of the pores allows for electroless deposition of metal. During the processing, the symmetry and the size of the nanopattern are conserved. The subsequent removal of the polymer template by pyrolysis leads to the formation of a inverse gyroid nickel nanofoam with porosity exceeding 50% v/v. The use of polymer templates with different compositions and sizes of the domains enabled us to further tune the porosity characteristics. Electromechanical properties of these nickel and other metal nanofoams will be investigated as part of our ongoing research.

EXPERIMENTAL SECTION

Materials. Four different diblock copolymers of polystyrene and poly(4-vinylpyridine) were obtained from Polymer Source Inc.: P9009-S4VP (M_n(PS) = 24 000 g mol^{-1}, M_n(P4VP) = 9500 g mol^{-1}, M_w/M_n = 1.10), P136-S4VP (M_n(PS) = 31 900 g mol^{-1}, M_n(P4VP) = 13 200 g mol^{-1}, M_w/M_n = 1.08), P5462-S4VP (M_n(PS) = 37 500 g mol^{-1}, M_n(P4VP) = 16 000 g mol^{-1}, M_w/M_n = 1.3), and P3912-S4VP (M_n(PS) = 41 500 g mol^{-1}, M_n(P4VP) = 17 500 g mol^{-1}, M_w/M_n = 1.07). The polymers were used as received. 3-Pentadecylphenol (PDP) was acquired from Aldrich (98 wt % purity) and was recrystallized twice from petroleum ether. Tin chloride (Acros Organics, anhydrous, 98%), palladium

chloride (Aldrich, 60% Pd basis), nickel sulfate (Aldrich, anhydrous, 99.99%), lactic acid (Aldrich, 85%), citric acid trisodium salt (Sigma-Aldrich, anhydrous), and borane dimethylamine complex (Aldrich, 97%) were used as received. The solvents were of analytical grade.

Preparation of Nanoporous Polymer Films. Films of the supramolecular complex were cast by dissolving the PS-*b*-P4VP diblock copolymer and PDP in chloroform. The concentration of polymer was kept below 2% to ensure homogeneous complex formation, and the solution was stirred for a couple of hours at room temperature. Afterward, the solution was poured into a glass Petri dish, which was subsequently placed into a saturated chloroform atmosphere. After several days, the chloroform was allowed to slowly evaporate, and subsequently the dish was heated for 20 min in an oven at 130 °C to make sure that the morphology represents the equilibrium structure of the melt state of the PS-*b*-P4VP(PDP) complex. The low molecular weight amphiphile was removed by stirring a piece of the film in ethanol for 3 days at room temperature, resulting in the formation of the nanoporous template for metal deposition.

Electroless Nickel Plating. The electroless metal plating technique that involved three steps was employed for Ni deposition onto the polymer substrate.[56,57] The first step was performed for surface sensitization. The nanoporous polymer film was immersed in an aqueous solution of tin chloride (0.1 M $SnCl_2$/0.1 M HCl), and the surface of the nanochannels adsorbed Sn^{2+}. After a thorough rinse with deionized water, the film was transferred into an aqueous solution of palladium chloride (0.0014 M $PdCl_2$/0.25 M HCl). In this step, the surface was activated by a redox reaction in which the Sn^{2+} ions were oxidized to Sn^{4+} and at the same time the Pd^{2+} ions were reduced to metallic Pd. This metallic palladium was used as the catalyst for the reduction of Ni^{2+}. After a thorough rinse with deionized water, Pd-containing films were immersed in an electroless nickel plating bath of the following composition: nickel sulfate (Ni source, 40 g L^{-1}), sodium citrate (complexant, 20 g L^{-1}), lactic acid (buffer, complexant, 10 g L^{-1}), and dimethyl amine borane (DMAB) (reductant, 1 g L^{-1}). The pH of the nickel bath was adjusted to 7.0 using ammonium hydroxide. Plating was done during 1 h at room temperature.

Formation of Nickel Nanofoam. The nickel-plated sample was kept in an oven (from 1 h up to 4 days) at 350 °C. This resulted in the degradation of the polymer template and exposure of the nickel network.

Characterization. Transmission electron microscopy was performed on a Philips CM10 transmission electron microscope operating at an accelerating voltage of 100 kV. Images are recorded on a Gatan slow-scan CCD camera. A piece of the film was embedded in an epoxy resin (Epofix, Electron Microscopy Sciences) and cured overnight at 40 °C. The sample was subsequently microtomed to a thickness of about 80 nm using a Leica Ultracut UCT-ultramicrotome and a diatome diamond knife at room temperature. The microtomed sections were floated on water and subsequently placed on copper grids. To obtain contrast during TEM, samples without metal were stained with iodine (45 h).

^{1}H NMR spectra in $CDCl_3$ were recorded on a 300 MHz Varian VXR operating at room temperature. The samples of the supramolecular complexes before and after PDP removal were prepared by dissolution of a piece of the film in $CDCl_3$.

Temperature-modulated differential scanning calorimetry was performed using a DSC Q1000 (TA Instruments). A modulated mode with heating/cooling rate of 1 °C min^{-1}, an oscillation amplitude of 0.5 °C, and an oscillation period of 60 s was used. Samples were first equilibrated at −30 °C, heated to 180 °C, cooled to −30 °C, and then heated again to 180 °C. Data taken from the second heating cycle were used for evaluation.

The nitrogen adsorption−desorption isotherms were determined on a Sorptomatic 1990 Thermo Finningen at 77 K. The sample was outgassed for 8 h at room temperature and for 18 h at 70 °C. The appropriate software (WinADP) and various models were used to analyze the obtained isotherms.[52,53,58,59] The specific surface area, S_{BET}, was calculated according to the Brunauer−Emmett−Teller (BET) method from the linear part of the nitrogen adsorption isotherm ($0.05 < p/p_0 < 0.25$). The pore size distribution was calculated according to the Dollimore and Heal method.

Mercury porosimetry was performed using a Carlo Erba 2000, software Milestone 200. The sample was dried at 50 °C for 8 h and degassed at room temperature and pressure of 0.5 Pa for 2 h. The total pore volume, V_p, and the average pore diameter, D, were acquired from cumulative pore distribution curve. The specific surface area, S_{Hg}, was calculated on the basis of the cylindrical pore model.[60,61]

TGA measurements were performed on a Perkin-Elmer thermogravimetric analyzer under the nitrogen atmosphere in a temperature range of 25−350 °C and with the heating rate of 20 °C min^{-1}.

Scanning electron microscopy and energy-dispersive analysis of X-rays were performed on a Philips XL-30S and XL-30 ESEM.

Acknowledgment. We thank Evgeny Polushkin for useful discussions. The authors acknowledge Gert Alberda van Ekenstein for TGA measurements, and Marc Stuart for his help with TEM.

Supporting Information Available: Additional figures and experimental details. This material is available free of charge *via* the Internet at http://pubs.acs.org.

REFERENCES AND NOTES

1. Tappan, B. C.; Steiner, S. A.; Luther, E. P. Nanoporous Metal Foams. *Angew. Chem., Int. Ed.* **2010**, *49*, 4544–4565.
2. Cammarata, R. C. Surface and Interface Stress Effects in Thin-Films. *Prog. Surf. Sci.* **1994**, *46*, 1–38.
3. Ibach, H. The Role of Surface Stress in Reconstruction, Epitaxial Growth and Stabilization of Mesoscopic Structures. *Surf. Sci. Rep.* **1997**, *29*, 195–263.
4. Weissmüller, J.; Viswanath, R. N.; Kramer, D.; Zimmer, P.; Würschum, R.; Gleiter, H. Charge Induced Reversible Strain in a Metal. *Science* **2003**, *300*, 312–315.
5. Kramer, D.; Viswanath, R. N.; Weissmüller, J. Surface-Stress Induced Macroscopic Bending of Nanoporous Gold Cantilevers. *Nano Lett.* **2004**, *4*, 793–796.
6. Baughman, R. H. Muscles Made from Metal. *Science* **2003**, *300*, 268–269.
7. Erlebacher, J.; Aziz, M. J.; Karma, A.; Dimitrov, N.; Sleradzki, K. Evolution of Nanoporosity in Dealloying. *Nature* **2001**, *410*, 450–453.
8. Brock, S. L.; Arachchige, I. U.; Mohanan, J. L. Porous Semiconductor Chalcogenide Aerogels. *Science* **2005**, *307*, 397–400.
9. Leventis, N.; Chandrasekaran, N.; Sadekar, A. G.; Sotiriou-Leventis, C.; Lu, H. One-Pot Synthesis of Interpenetrating Inorganic/Organic Networks of CuO/Resorcinol-Formaldehyde Aerogels: Nanostructured Energetic Materials. *J. Am. Chem. Soc.* **2009**, *131*, 4576–4577.
10. Varma, A.; Rogachev, A. S.; Mukasyan, A. S.; Hwang, S. Combustion Synthesis of Advanced Materials: Principles and Applications. *Adv. Chem. Eng.* **1998**, *24*, 79–226.
11. Ashby, M. F.; Evans, A. G.; Fleck, N. A.; Gibson, L. J.; Hutchinson, J. W.; Wadley, H. G. *Metal Foams: A Design Guide*; Butterworth-Heinemann: Oxford, UK, 2000.
12. Tekoglu, C. Size Effects in Cellular Solids. Ph.D. Thesis, University of Groningen, 2007.
13. Amsterdam, E. Structural Performance and Failure Analysis of Aluminium Foams. Ph.D. Thesis, University of Groningen, 2008.
14. Bates, F. S.; Fredrickson, G. H. Block Copolymer Thermodynamics: Theory and Experiment. *Annu. Rev. Phys. Chem.* **1990**, *41*, 525–527.
15. Hamley, I. W. *The Physics of Block Copolymers*; Oxford University Press: Oxford, 1998.
16. Abetz, V.; Simon, P. F. W. Phase Behaviour and Morphologies of Block Copolymers. *Adv. Polym. Sci.* **2005**, *189*, 125.
17. Hajduk, D. A.; Harper, P. E.; Gruner, S. M.; Honeker, C. C.; Kim, G.; Thomas, E. L.; Fetters, L. J. The Gyroid: A New Equilibrium Morphology in Weakly Segregated Diblock Copolymers. *Macromolecules* **1994**, *27*, 4063–4075.

18. Schulz, M. F.; Bates, F. S.; Almdal, K.; Mortensen, K. Epitaxial Relationship for Hexagonal-to-Cubic Phase Transition in a Block Copolymer Mixture. *Phys. Rev. Lett.* **1994**, *73*, 86–89.
19. Urbas, A. M.; Maldovan, M.; DeRege, P.; Thomas, E. L. Bicontinuous Cubic Block Copolymer Photonic Crystals. *Adv. Mater.* **2002**, *14*, 1850–1853.
20. Davidock, D. A.; Hillmyer, M. A.; Lodge, T. P. Persistence of the Gyroid Morphology at Strong Segregation in Diblock Copolymers. *Macromolecules* **2003**, *36*, 4682–4685.
21. Cochran, E. W.; Garcia-Cervera, C. J.; Fredrickson, G. H. Stability of the Gyroid Phase in Diblock Copolymers at Strong Segregation. *Macromolecules* **2006**, *39*, 2449–2451.
22. Bates, F. S.; Fredrickson, G. H. Block Copolymers—Designer Soft Materials. *Phys. Today* **1999**, *52*, 32–38.
23. Epps, T. H., III; Cochran, E. W.; Bailey, T. S.; Waletzko, R. S.; Hardy, C. M.; Bates, F. S. Ordered Network Phases in Linear Poly(isoprene-*b*-styrene-*b*-ethylene oxide) Triblock Copolymers. *Macromolecules* **2004**, *37*, 8325–8341.
24. Tyler, C. A.; Qin, J.; Bates, F. S.; Morse, D. C. SCFT Study of Nonfrustrated ABC Triblock Copolymer Melts. *Macromolecules* **2007**, *40*, 4654–4668.
25. Fleury, G.; Bates, F. S. Perpendicular Lamellae in Parallel Lamellae in a Hierarchical CECEC-P Hexablock Terpolymer. *Macromolecules* **2009**, *42*, 1691–1694.
26. Masuda, J.; Takano, A.; Nagata, Y.; Noro, A.; Matsushita, Y. Nanophase-Separated Synchronizing Structure with Parallel Double Periodicity from an Undecablock Terpolymer. *Phys. Rev. Lett.* **2006**, *97*, 098301.
27. Matsushita, Y. Creation of Hierarchically Ordered Nanophase Structures in Block Polymers Having Various Competing Interactions. *Macromolecules* **2007**, *40*, 771–776.
28. Hillmyer, M. A. Nanoporous Materials from Block Copolymer Precursors. *Adv. Polym. Sci.* **2005**, *190*, 137–181.
29. Park, S.; Wang, J. Y.; Kim, B.; Xu, J.; Russell, T. P. A Simple Route to Highly Oriented and Ordered Nanoporous Block Copolymer Templates. *ASC Nano* **2008**, *2*, 766–772.
30. Crossland, E. J. W.; Kamperman, M.; Nedelcu, M.; Ducati, C.; Wiesner, U.; Smilgies, D. M.; Toombes, G. E. S.; Hillmyer, M. A.; Ludwigs, S.; Steiner, U.; *et al.* A Bicontinuous Double Gyroid Hybrid Solar Cell. *Nano Lett.* **2009**, *9*, 2807–2812.
31. Joo, W.; Yang, S. Y.; Kim, J. K.; Jinnai, H. Nanohole Structure Prepared by a Polystyrene-*block*-Poly(methyl methacrylate) /Poly(methyl methacrylate) Mixture Film. *Langmuir* **2008**, *24*, 12612–12617.
32. Mansky, P.; Harrison, C. K.; Chaikin, P. M.; Register, R. A.; Yao, N. Nanolithographic Templates from Diblock Copolymer Thin Films. *Appl. Phys. Lett.* **1996**, *68*, 2586–2588.
33. Chen, S. Y.; Huang, Y.; Tsiang, R. C. Ozonolysis Efficiency of PS-*b*-PI Block Copolymers for Forming Nanoporous Polystyrene. *J. Polym. Sci., Part A: Polym. Chem.* **2008**, *46*, 1964–1973.
34. Mäki-Ontto, R.; de Moel, K.; de Odorico, W.; Ruokolainen, J.; Stamm, M.; ten Brinke, G.; Ikkala, O. "Hair Tubes": Mesoporous Materials Containing Hollow Self-Organized Cylinders with Polymer Brushes at the Walls. *Adv. Mater.* **2001**, *13*, 117–121.
35. Ikkala, O.; ten Brinke, G. Functional Materials Based on Self-Assembly of Polymeric Supramolecules. *Science* **2002**, *295*, 2407–2409.
36. Nandan, B.; Vyas, M. K.; Böhme, M.; Stamm, M. Composition-Dependent Morphological Transitions and Pathways in Switching of Fine Structure in Thin Films of Block Copolymer Supramolecular Assemblies. *Macromolecules* **2010**, *43*, 2463–2473.
37. Thurn-Albrecht, T.; Schotter, J.; Kästle, G. A.; Emley, N.; Shibauchi, T.; Krusin-Elbaum, L.; Guarini, K.; Black, C. T.; Tuominen, M. T.; Russell, T. P. Ultrahigh-Density Nanowire Arrays Grown in Self-Assembled Diblock Copolymer Templates. *Science* **2000**, *290*, 2126–2129.
38. Sidorenko, A.; Tokarev, I.; Minko, S.; Stamm, M. Ordered Reactive Nanomembranes/Nanotemplates from Thin Films of Block Copolymer Supramolecular Assembly. *J. Am. Chem. Soc.* **2003**, *125*, 12211–12216.
39. Jeong, U.; Kim, H. C.; Rodriguez, R. L.; Tsai, I. Y.; Stafford, C. M.; Kim, J. K.; Hawker, C. J.; Russell, T. P. Asymmetric Block Copolymers with Homopolymers: Routes to Multiple Length Scale Nanostructures. *Adv. Mater.* **2002**, *14*, 274–276.
40. Mao, H.; Hillmyer, M. A. Macroscopic Samples of Polystyrene with Ordered Three-Dimensional Nanochannels. *Soft Matter* **2006**, *2*, 57–59.
41. Hashimoto, T.; Tsutsumi, K.; Funaki, Y. Nanoprocessing Based on Bicontinuous Microdomains of Block Copolymers: Nanochannels Coated with Metals. *Langmuir* **1997**, *13*, 6869–6872.
42. Hashimoto, T.; Nishikawa, Y.; Tsutsumi, K. Identification of the "Voided Double-Gyroid-Channel": A New Morphology in Block Copolymers. *Macromolecules* **2007**, *40*, 1066–1072.
43. Urade, V. N.; Wei, T. C.; Tate, M. P.; Kowalski, J. D.; Hillhouse, H. W. Nanofabrication of Double-Gyroid Thin Films. *Chem. Mater.* **2007**, *19*, 768–777.
44. Gobius du Sart, G.; Vuković, I.; Vuković, Z.; Polushkin, E.; Hiekkataipale, P.; Ruokolainen, J.; Loos, K.; ten Brinke, G. Nanoporous Network Channels from Self-Assembled Triblock Copolymer Supramolecules. *Macromol. Rapid Commun.* **2011**, *32*, 366–370.
45. Alberda van Ekenstein, G. O. R.; Meyboom, R.; ten Brinke, G.; Ikkala, O. Determination of the Flory—Huggins Interaction Parameter of Styrene and 4-Vinylpyridine Using Copolymer Blends of Poly(styrene-*co*-4-vinylpyridine) and Polystyrene. *Macromolecules* **2000**, *33*, 3752–3756.
46. Zha, W.; Han, C. D.; Lee, D. H.; Han, S. H.; Kim, J. K.; Kang, J. H.; Park, C. Origin of the Difference in Order—Disorder Transition Temperature between Polystyrene-*block*-poly(2-vinylpyridine) and Polystyrene-*block*-poly(4-vinylpyridine) Copolymers. *Macromolecules* **2007**, *40*, 2109–2119.
47. Matsen, M. W.; Schick, M. Stable and Unstable Phases of a Diblock Copolymer Melt. *Phys. Rev. Lett.* **1994**, *72*, 2660–2663.
48. Polushkin, E.; Alberda van Ekenstein, G. O. R.; Knaapila, M.; Ruokolainen, J.; Torkkeli, M.; Serimaa, R.; Bras, W.; Dolbnya, I.; Ikkala, O.; ten Brinke, G. Intermediate Segregation Type Chain Length Dependence of the Long Period of Lamellar Microdomain Structures of Supramolecular Comb—Coil Diblocks. *Macromolecules* **2001**, *34*, 4917–4922.
49. Finnefrock, A. C.; Ulrich, R.; Toombes, G. E. S.; Gruner, S. M.; Wiesner, U. The Plumber's Nightmare: A New Morphology in Block Copolymer—Ceramic Nanocomposites and Mesoporous Aluminosilicates. *J. Am. Chem. Soc.* **2003**, *125*, 13084–13093.
50. Valkama, S.; Ruotsalainen, T.; Nyka1nen, A.; Laiho, A.; Kosonen, H.; ten Brinke, G.; Ikkala, O.; Ruokolainen, J. Self-Assembled Structures in Diblock Copolymers with Hydrogen-Bonded Amphiphilic Plasticizing Compounds. *Macromolecules* **2006**, *39*, 9327–9336.
51. Kobayashi, Y.; Tadaki, Y.; Nagao, D.; Konno, M. Deposition of Gold Nanoparticles on Polystyrene Spheres by Electroless Metal Plating Technique. *J. Phys.: Conf. Ser.* **2007**, *61*, 582–586.
52. Gregg, S. H.; Sing, K. S. *Adsorption, Surface Area and Porosity*; Academic Press: New York, 1967.
53. Rouquerol, F.; Rouquerol, J.; Sing, K. *Adsorption by Powders and Porous Solids*; Academic Press: London, 1999.
54. Lee, I.; Hammond, P. T.; Rubner, M. F. Selective Electroless Nickel Plating of Particle Arrays on Polyelectrolyte Multilayers. *Chem. Mater.* **2003**, *15*, 4583–4589.
55. Boontongkong, Y.; Cohen, R. E.; Rubner, M. F. Selective Electroless Copper Deposition within Block Copolymer Microdomains. *Chem. Mater.* **2000**, *12*, 1628–1633.
56. Mallory, G. O.; Hajdu, J. B. *Electroless Plating: Fundamentals and Applications*, American Electroplaters and Surface Finishers Society, 1992.
57. Riedel, W., Ed. *Electroless Nickel Plating*; Finishing Publications: Metals Park, OH, 1991.
58. Sing, K.; Everett, D.; Haul, R.; Moscou, L.; Perolti, R.; Rouguerol, J.; Siemieniewska, T. Repoting Physisorption Data for Gas/Solid Systems with Special Reference to the Determination of Surface Area and Porosity. *Pure Appl. Chem.* **1985**, *57*, 603–619.

59. Dollimore, D.; Heal, G. R. An Improved Method for the Calculation of Pore Size Distribution from Adsorption Data. *J. Appl. Chem.* **1964**, *14*, 109–114.
60. Webb, P. A.; Orr, C. *Analytical Methods in Fine Particle Technology*; Micrometrics Instrument Corporation: Norcross, GA, 1997.
61. Leofanti, G.; Padovan, M.; Tozzola, G.; Venturelli, B. Surface Area and Pore Texture of Catalysts. *Catal. Today* **1998**, *41*, 207–219.